Environmental Science and Pollution Research (2024) 31:29132–29147
https://doi.org/10.1007/s11356-024-32838-5

RESEARCH ARTICLE

Efficient phosphate removal by Mg-La binary layered double hydroxides: synthesis optimization, adsorption performance, and inner mechanism

Yanming Xu[1] · Yue Yin[1] · Ya-Nan Luan[1] · Qing Wang[1] · Zhuo Zhao[1] · Zhonghong Guo[1] · Changqing Liu[1]

Received: 8 November 2023 / Accepted: 5 March 2024 / Published online: 3 April 2024

Abstract

Layered double hydroxides (LDH) hold great promise as phosphate adsorbents; however, the conventional binary LDH exhibits low adsorption rate and adsorption capacity. In this study, Mg and La were chosen as binary metals in the synthesis of Mg-La LDH to enhance phosphate efficient adsorption. Different molar ratios of Mg to La (2:1, 3:1, and 4:1) were investigated to further enhance P adsorption. The best performing Mg-La LDH, with Mg to La ratio is 4:1 (LDH-4), presented a larger adsorption capacity and faster adsorption rate than other Mg-La LDH. The maximum adsorption capacity (87.23 mg/g) and the rapid adsorption rate in the initial 25 min of LDH-4 (70 mg/(g·h)) were at least 1.6 times and 1.8 times higher than the others. The kinetics, isotherms, the effect of initial pH and co-existing anions, and the adsorption-desorption cycle experiment were studied. The batch experiment results proved that the chemisorption progress occurred on the single-layered LDH surface and the optimized LDH exhibited strong anti-interference capability. Furthermore, the structural characteristics and adsorption mechanism were further investigated by SEM, BET, FTIR, XRD, and XPS. The characterization results showed that the different metal ratios could lead to changes in the metal hydroxide layer and the main ions inside. At lower Mg/La ratios, distortion occurred in the hydroxide layer, resulting in lower crystallinity and lower performance. The characterization results also proved that the main mechanisms of phosphate adsorption are electrostatic adsorption, ion exchange, and inner-sphere complexation. The results emphasized that the Mg-La LDH was efficient in phosphate removal and could be successfully used for this purpose.

Keywords Phosphate removal · Adsorption · Mg-La LDH · Metal ratio · chemisorption · Ion exchange

Introduction

Phosphorus is an essential nutrient for all living organisms whereas its excessive presence in natural water bodies has gradually become a global environmental problem (Cordell et al. 2009). The major status of phosphorus in natural water bodies and wastewater is phosphate (P). The phosphorus concentration higher than 0.02 mg/L would lead to the eutrophication of biological systems (Yin et al. 2021). The US Environmental Protection Agency (US-EPA) requires the total phosphorus limit in surface water (river, lake) to be 0.02 to 0.1 mg/L (Liu et al. 2021). The demand for phosphorus removal in water treatment facilities is steadily increasing, necessitating the development of a cost-effective and efficient technology for phosphorus removal. As a typical phosphorus removal process, adsorption technology exhibits better performance than other processes and has been widely accepted for phosphorus

Highlights
- The Mg-La LDH powder was successfully synthesized by the traditional co-precipitation method.
- The Mg/La ratio of 4:1 in the preparation of Mg-La LDH results in high affinity to P due to the excellent crystallinity and stable lamellar structure.
- The maximum adsorption capacity for P can reach 81.96 mg/g when the equilibrium concentration is 0.5 mg/g.
- The adsorption mechanism involved electrostatic attraction, ion exchange, and complexation.
- Mg-La LDH possibly emerged as the promising material for the effective removal of P from water.

Responsible Editor: Tito Roberto Cadaval Jr

✉ Changqing Liu
lcqfyqut@126.com

[1] School of Environmental and Municipal Engineering, Qingdao University of Technology, Qingdao 266520, China

removal from water/wastewater, especially for low-concentration phosphorus removal due to its high efficiency, low energy consumption, and flexibility (El-Qelish et al. 2024; Xiong et al. 2017).

In water treatment, commonly employed adsorbents for phosphate removal includes activated carbon and biochar (Chen et al. 2023), metal oxides (Lin et al. 2019a; Lin et al. 2019b), waste modified material (Qiao et al. 2022; Yin et al. 2021), clay, chitosan-based materials (Feng et al. 2022a), montmorillonite (Zou et al. 2020), porous silicon dioxide (Shin et al. 2004), and layered double hydroxides (LDH) (Feng et al. 2022a). Among these adsorbents, LDH, a versatile ionic layered compound, has been considered a promising adsorbent for phosphorus removal. The composition elements and preparation conditions of these compounds can be fine-tuned over a broad range, thereby imparting them with a highly adjustable hydrotalcite structure. Previous studies have proposed many LDH in P removal; the P adsorption capacity of Mg Al LDH prepared by co-precipitation method such as Dox et al. (Dox et al. 2019) was 61 mg/g. The Mg Al LDH prepared by Ribeiro et al. (2023) could complete the adsorption in 60 min. These can fully demonstrate the high efficiency of LDH for P adsorption in water. However, it is worth noting that the high P adsorption capacity of binary LDH in most studies was due to the extremely high initial P concentrations (100–500 mg/L), whereas P concentrations often fluctuated around 5–10 mg/L in real-world wastewater. A high initial P concentration would not only inevitably lead to high adsorption capacity but also result in a high remaining concentration of P (~ 50 mg/L). Therefore, the theoretical adsorption capacity derived from this scenario would not be applicable in real applications. Consequently, the synthesis of binary LDH should be further optimized for better P adsorption performance.

Previous reports have demonstrated that the element La could be used as an efficient functional material in adsorption which exhibits a strong affinity for phosphate and possesses low toxicity and chemical stability (Koilraj and Sasaki 2017; Wu et al. 2007). For instance, the P adsorption capacity of lanthanum hydroxide and lanthanum carbonate prepared by Wu et al. (2022) could achieve efficient adsorption performance at low P equilibrium concentrations. It was hypothesized that the incorporation of La in LDH synthesis would also exhibit commendable P adsorption performance. However, there is a scarcity of studies on the synthesis of efficient binary LDHs with La.

The present study reported the successful synthesis of a novel Mg-La LDH via the traditional co-precipitation method. This study aimed to fabricate a novel binary LDH using Mg and La to achieve efficient adsorption performance at low P equilibrium concentrations. The optimum preparation conditions of Mg-La LDH were determined through single-factor analysis and comparison of adsorption capacity. The effects of kinetics, adsorption isotherms, and solution pH were investigated to confirm the optimal ratio of Mg and La. Various isotherm and kinetic models for the adsorption and interaction between the P and Mg-La LDH were applied. Subsequently, the potential for phosphorus removal and the regeneration possibility of Mg-La LDH on actual wastewater was assessed by examining the impact of coexisting ions and conducting cyclic desorption experiments. Finally, the changes in structure and chemical composition of Mg-La LDH before and after phosphate adsorption were investigated by means of SEM, XRD, FTIR, and XPS. The underlying adsorption mechanism of this composite material was further discussed.

Materials and methods

Materials

Magnesium chloride ($MgCl_2{\cdot}6H_2O$), lanthanum chloride ($LaCl_3{\cdot}7H_2O$), ferric chloride ($FeCl_3$), aluminum chloride ($AlCl_3$), hydrochloric acid (HCl), sodium hydroxide (NaOH), and potassium dihydrogen phosphate (KH_2PO_4) were purchased from Sinopharm Chemical Reagent Co, Ltd. (Shanghai, China). A stock solution of phosphorous was prepared by dissolving 4.394 g of KH_2PO_4 in 1000 mL of deionized water. In addition, phosphate solutions of different concentrations were prepared by diluting the stock solution. All chemicals used in this study were of analytical grade.

Synthesis of LDH powder

Mg-La LDH powder was synthesized by the traditional co-precipitation method (Li et al. 2022; Zhang et al. 2021c). Specifically, $MgCl_2{\cdot}6H_2O$ and $LaCl_3{\cdot}7H_2O$ were added into 150 mL deionized water to prepare a mixed solution with the Mg^{2+}:La^{3+} molar ratio of 2:1, 3:1, and 4:1, respectively. Then, under stirring, 1.0 mol/L NaOH solution was slowly added to the above solution to adjust the pH to 10. After stirring for 30 min, this reaction mixture was further aged for 10 h at 80 °C. The final precipitate was washed with deionized water and dried in an oven at 80 °C. The adsorbents were named LDH-X, where the *X* represents the ratio of Mg^{2+}:La^{3+}. According to the above method, the LDH-Fe (Mg^{2+}:Fe^{3+} molar ratio of 2:1) and LDH-Al (Mg^{2+}:Al^{3+} molar ratio of 2:1) were synthesized (Fig. 1).

Batch experiments

A series of batch experiments were carried out to investigate and compare the adsorbents by figuring out the effect of adsorption time, P concentration, and pH on the adsorption

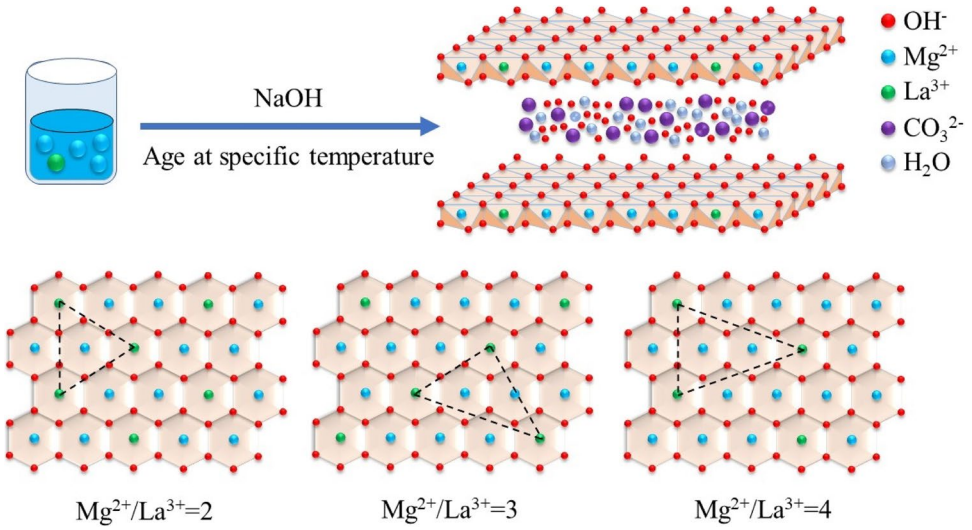

Fig. 1 Schematic illustration for the preparation of Mg-La LDH by co-precipitation and the structure of them

capacity. All adsorption experiments were performed at room temperature (25 °C) with the same adsorption dose (0.4 g/L). The P after the reaction was determined by the ascorbic method (APHA. 2017) and detected by a UV-spectrophotometer (HACH, DR2800) at 700 nm. To make the data reliable, three parallel samples were used for each experiment, and the data were average value.

The equilibrium adsorption capacity (q_e) and the removal rate (R) of phosphate were calculated using the following equation:

$$q_e = \frac{(C_0 - C_e)V}{m} \tag{1}$$

$$R = \frac{(C_0 - C_e)}{C_0} * 100\% \tag{2}$$

where C_0 and C_e (mg/L) are the initial and equilibrium concentrations, m (g) is the mass of adsorbent, and V (L) is the volume of the solution.

Adsorption models

The adsorption data in this study was fitted by the kinetic models and adsorption isotherms for further interpretation. Three adsorption kinetics, pseudo-first-order model, pseudo-second-order model, and intraparticle diffusion model were represented by Eqs. (3) to (5), respectively (Li et al. 2021a).

$$\ln(q_e - q_t) = \ln q_e - K_1 t \tag{3}$$

$$\frac{t}{q_t} = \frac{1}{K_2 {q_e}^2} + \frac{t}{q_e} \tag{4}$$

$$q_t = k_i t^{\frac{1}{2}} + I \tag{5}$$

where q_t (mg/g) is the adsorption capacity at time t, K_1 (min^{-1}) and K_2 (g/(mg·min)) are the adsorption rate constant of pseudo-first-order and pseudo-second-order, k_i (mg/(g·$h^{1/2}$)) is the adsorption rate constant of the intraparticle diffusion model, and the I (mg/g) is the constant associated with the boundary layer reaction.

The adsorption isotherms such as Langmuir isotherm and Freundlich isotherm were used in this study (Yang et al. 2022). Both models can be expressed as Eqs. (6) and (7):

$$q_e = \frac{q_m K_L C_e}{1 + K_L C_e} \tag{6}$$

$$q_e = K_F {C_e}^{1/n} \tag{7}$$

where q_m (mg/g) represents the theoretical maximum adsorption capacity of the adsorbent and K_L (L/mg) is the equilibrium constant related to the binding energy. The K_F (mg/g) is the Freundlich adsorption capacity, and the n is the Freundlich constant which has a higher value for a less heterogeneous surface. Furthermore, the dimensionless factor R_L is defined by Eq. (8):

$$R_L = \frac{1}{1 + K_L C_0} \tag{8}$$

The adsorption nature is irreversible at $R_L = 0$, favorable at $0 < R_L < 1$, or unfavorable at $R_L > 1$ (Li et al. 2023).

Characterization of the adsorbents

The surface morphology of the adsorbent was analyzed by scanning electron microscopy (SEM) (Hitachi, S-4800),

and the crystal structure of the adsorbent was analyzed via X-ray diffraction (XRD) (Bruker, D8 ADVANCE). The analysis was based on the Bragg equation (Santos et al. 2020), which established a relationship between the intensity of diffraction peaks and the angle of incidence as well as the spacing of the lattice, as follows:

$$n\lambda = 2d\sin\theta \tag{9}$$

where d (Å) is the lamella distance, n is the reflection order of the peak, λ (Å) is the wavelength of the ray, and θ (°) is the Bragg Angle determined by the peak diffraction.

The adsorption and desorption of N_2 by the adsorbent were characterized using Brunauer-Emmett-Teller (BET) (Quantachrome Instruments, Autosorb-iQ) methods to determine the specific surface area. The thermal stability of solid samples was determined using thermogravimetric analysis (TG) (HITACHI STA200). Fourier transform infrared spectra (FTIR) (Nicolet, 6700) was employed to characterize the characteristic functional groups of the adsorbent before and after phosphorus removal, while energy dispersive X-ray photoelectron spectroscopy (XPS) (Thermo Scientific, K-Alpha X) was utilized to analyze the elements of the adsorbent before and after adsorption, thereby facilitating further discussion on the adsorption mechanism.

Mg-La LDH regeneration

To explore the reusability of Mg-La LDH, an adsorption-desorption cycle experiment was carried out. In this study, the optimal desorption solution was determined by single-factor analysis. Based on the results and extensive literature research, Na_2CO_3 was identified as a suitable desorbing agent for LDH, Therefore, sodium carbonate was used for desorption purposes. The desorption solution was supplemented with the adsorbent after the adsorption of phosphorus, and the concentration of phosphate in the desorption solution was determined to calculate the desorption rate. Subsequently, adsorption experiments were performed to evaluate the reuse performance through an adsorption-desorption cycle.

Results and discussion

Synthesis optimization

In the process of preparing LDH, in order to obtain a stable lamination structure, metal cations with little difference in ionic radii (0.065~0.080 nm) were generally used as layered structures, and the ratio of divalent and trivalent metal cations was controlled to be 2–4 (Feng et al. 2022b). The radii of Mg and La ions used in this paper were not similar, so the synthesis ratio and preparation conditions had higher requirements. Based on previous research (Zubair et al. 2017; Daud et al. 2019), the reaction temperature, reaction pH, and reaction time were three significant operational parameters that exhibited great influences on the properties and structure of LDH. Therefore, in this study, the effect of these three parameters was first investigated.

As given in Fig. 2(a, b), increasing the synthesis temperature and extending the synthesis time within an appropriate range can help improve the P removal. However, excessive heating time led to a slight decrease in the adsorption effect. This was because the primary laminate formed in the early stage could not form a well-crystallizable LDH structure at a low synthesis temperature and time, resulting in a poor adsorption effect. The increase in temperature facilitated the morphological transformation of LDH, leading to a gradual enhancement in the crystallinity of LDH structure. Consequently, this promoted the formation of LDH with a well-developed crystal structure and abundant pores, thereby enhancing its adsorption capacity (Iqbal and Fedel 2018). However, excessive temperature or prolonged synthesis time can lead to gradual degradation of the LDH structure, resulting in reduced crystallinity and subsequent formation of other phases, ultimately leading to a decrease in adsorption capacity.

As shown in Fig. 2c, an increase in pH within the appropriate range helped to improve the removal of P, but if the pH was above 12, the effect would slightly decrease. This was because the primary laminates could not be formed well at low pH, so the LDH structure was not formed during subsequent heating and aging, resulting in poor adsorption capacity (Bukhtiyarova 2019). When the pH was excessively high, on the one hand, the formation of LDH layer structure would be unstable during heating aging, leading to easy precipitation of metal ions and their transformation into metal hydroxide precipitates, thereby resulting in poor crystallinity of LDH. On the other hand, it would lead to the increase of Na ions in the solution, so that the Na phase may appear in the LDH structure, resulting in the instability of the LDH structure. Both aspects ultimately contribute to diminished adsorption capabilities. According to the results of the single-factor analysis, the optimum synthesis parameters were determined as follows: synthesis temperature of 80 °C, synthesis pH of 10, and synthesis time of 10 h, and these parameters were used in the following experiments.

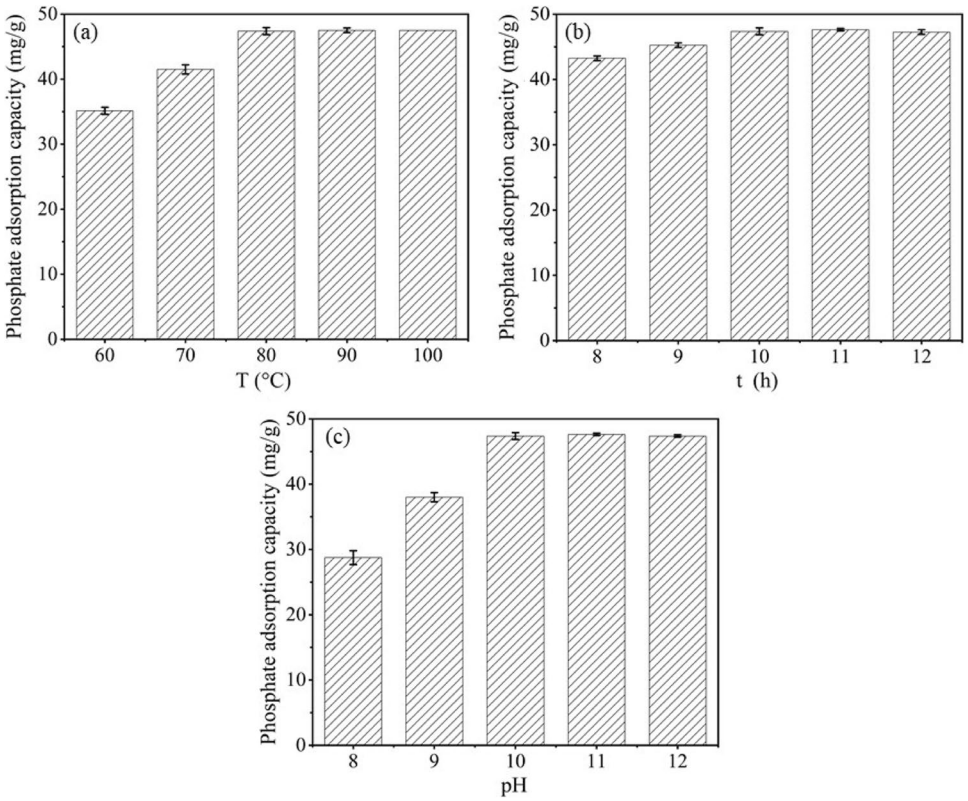

Fig. 2 The effect of reaction temperature (**a**), reaction time (**b**), and reaction pH (**c**) on the P adsorption performance of LDH-4

Characterization of the adsorbents

To characterize the morphology of the synthesized Mg-La LDH, the SEM images of Mg-La LDH with different molar ratios of Mg/La are given in Fig. 3. All three LDH samples exhibited uniform particle size, smooth surface topography, abundant porosity, and compact structure. This suggested that the successful synthesis of Mg-La LDH particles was not easily affected by different molar ratios of Mg/La. However, through comparison, it was evident that LDH-4 (Fig. 3c, f) possessed a more obvious crystal structure on the surface, smoother surface texture, and superior crystallinity than the other two LDHs.

The FTIR spectra of three LDHs are shown in Fig. 4a. A sharp peak at 3694 cm^{-1} corresponded to hydroxyl stretching resulting from the presence of interlayer water and hydroxyl groups (Cavani et al. 1991). The stretching vibration at 3435 cm^{-1} represented O-H, and the bending vibration at 1441 and 1439 cm^{-1} corresponded to O-H as well. The vibrational bands at 856 cm^{-1} and in the range of 700–724 cm^{-1} were attributed to the Mg-La LDH interlayer carbonate anion group, specifically corresponding to the carbonate v_2 and v_4 vibrations, respectively (Li et al. 2023). It was noteworthy that LDH-4 exhibited a low intensity in the vibration zone of 856 cm^{-1} and only displayed a single peak in 700–724 cm^{-1}. This observation suggested a limited presence of CO_3^{2-}, thereby indicating that the internal anion of LDH-4 exhibits a higher concentration of OH^-. That may be attributed to the different composition and irregular ordering of internal anions caused by different metal ratios. Moreover, the peaks observed at 1487 and 1484 cm^{-1} represented La-O bonding interactions, whereas that detected at 651 cm^{-1} was the tensile vibration associated with M-O and M-O-M (M represents Mg or La) (Santosa et al. 2008). Overall, these results of FTIR confirmed that the structure of the three LDHs consisted primarily of metal hydroxide layers with intermediate layers composed of both hydroxide and carbonate anions.

The crystal phase results (Fig. 4b) demonstrated that Mg-La LDH exhibited four distinct diffraction peaks at 2θ = 11.6° (003), 23.5° (006), 34.1° (009), and 39.3° (015). These peaks corresponded to the characteristic LDH structure, confirming the successful formation of a layered double hydroxide structure (Isidoro Ribeiro et al. 2023). Three additional crystalline phases $La(OH)_3$, $LaCO_3OH$, and $Mg(OH)_2$ were observed in the Mg-La LDH system. Among them, LDH-4 was predominantly composed of $La(OH)_3$ while the other two were dominated by $LaCO_3OH$. This observation was consistent with the weak CO_3^{2-} peak observed in LDH-4 using FTIR spectroscopy. On one hand, this can be attributed to the limited remote ordering ability resulting from the strong Jahn-Teller effect resulting from the extended M-O distance (Cavani et al. 1991). On the other hand, it

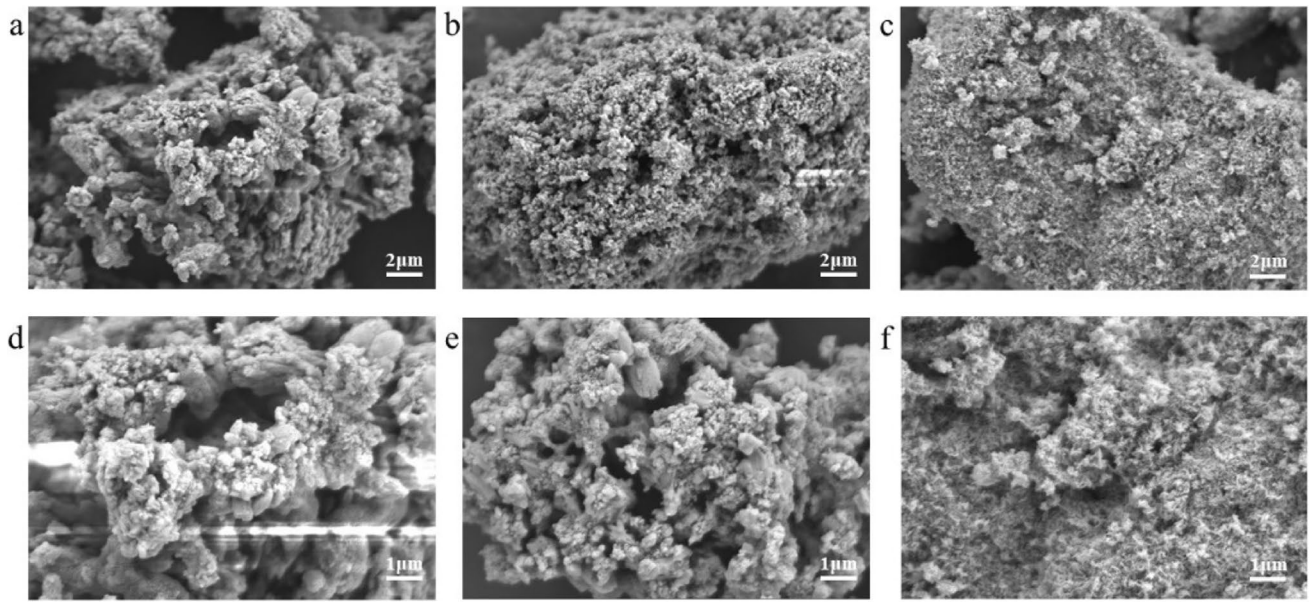

Fig. 3 SEM images of LDH-2 (**a**, **d**), LDH-3 (**b**, **e**), and LDH-4 (**c**, **f**)

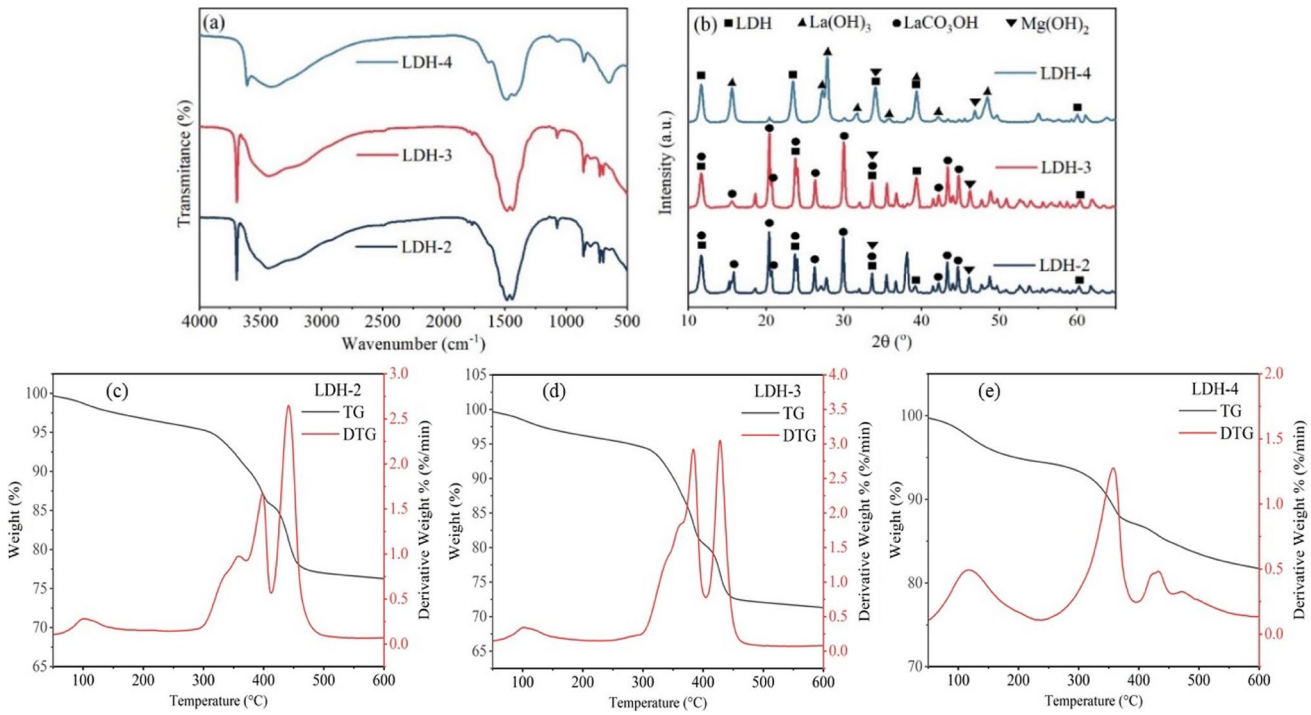

Fig. 4 FTIR spectra (**a**), XRD patterns (**b**), and TG-DTG analysis (**c**–**e**) of Mg-La LDHs

may also be influenced by differences in assembly due to varying metal ratios.

According to the formula calculation, all LDH crystal parameters are presented in Table 1. It can be observed that the surface spacing (d_{003}) of LDH-2, LDH-3, and LDH-4 is 7.60 Å, 7.58 Å, and 7.57 Å, respectively. Notably, LDH-4 exhibited the smallest value which further substantiated that OH^- predominantly constituted the middle layer anion of LDH-4. The d_{003} layer spacing of LDH-4 closely approximated twice that of d_{006} layer spacing, indicating that Mg:La = 4:1 synthesis yields a lamellar structure with superior crystallinity among other ratios tested (Ookubo et al. 1992; Bukhtiyarova 2019). This was further supported by the crystal parameters *a* and *c*, both exhibiting their maximum

Table 1 Crystallographic parameters of Mg-La LDH

Parameter	LDH-2	LDH-3	LDH-4
d_{003}	7.60	7.58	7.57
d_{006}	3.76	3.75	3.78
$a = 2d_{110}$	3.07	3.07	3.08
$c = 3(d_{003} + d_{006})/2$	22.68	22.62	22.70

values when the Mg:La=4:1 ratio was employed, suggesting its favorable conditions for nucleation and growth resulting in highly crystalline LDH formation. This phenomenon may be attributed to the difference in ionic radii between Mg and La ions; at lower Mg/La ratios, distortion occurs within the hydroxide layer leading to reduced crystallinity and inferior properties (Ahmed et al. 2012).

TG-DTA measurements were performed to elucidate the thermophysical changes across endothermic and exothermic effects. Figure 4 (c–e) demonstrated the TG-DTA graphs (50–800 °C) of LDH-2, LDH-3, and LDH-4, respectively. In this study, the first weight loss occurred at about 120 °C. This weight loss can be attributed to the removal of the H_2O molecule s as well as the dehydration of interlayer species in Mg-La LDH (Wang et al. 2016; Maged et al. 2023a). The high temperature region between 250 and 450 °C had been attributed to the decomposition of LDH (Tang et al. 2018). Notably, LDH-4 had the smallest weight loss, which indicated that LDH-4 had a more crystalline and stable structure.

Adsorption kinetics

In order to investigate the adsorption rate of these LDHs, adsorption kinetics experiments were carried out. As shown in Fig. 5a, in the initial 60 min, a high adsorption rate can be observed, with the adsorption capacity reaching more than 70% of the equilibrium (specifically, LDH-2 is 71%, LDH-3 is 70%, and LDH-4 is 90%). This finding demonstrated the rapid phosphate removal performance of Mg-La LDH from water, especially for LDH-4. As the adsorption process proceeded, the number of active sites on different LDHs decreased gradually, resulting in relatively slower adsorption progress afterward. Under the condition of initial P of 10 mg/L, dosage of 0.4 g/L, and initial pH of 7, it took around 12 h for all three types of LDH to reach equilibrium, achieving adsorption performance of 15.88 mg/g, 19.25 mg/g, and 25.00 mg/g, for LDH-2, LDH-3, and LDH-4, respectively. On the contrary, conventional LDHs (LDH-Al and LDH-Fe) exhibited poor adsorption capacity. Furthermore, the

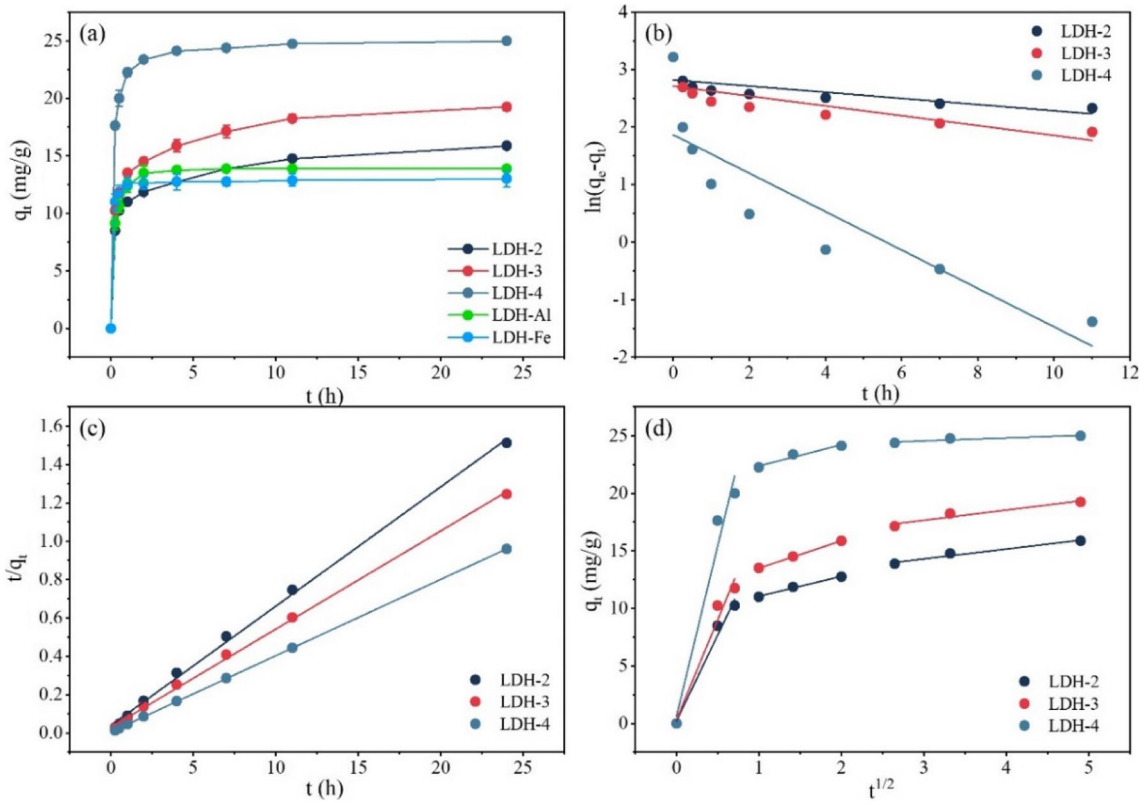

Fig. 5 10 mg/g concentration curve (**a**), pseudo-first-order model (**b**), pseudo-second-order model (**c**), and intraparticle diffusion model (**d**) for the adsorption of phosphate

complete removal of P from water by LDH-4 within 12 h further demonstrated the high efficiency of Mg-La LDH.

To further interpret the adsorption data, different kinetic models were used and fitted. As given in Table 2, the R^2 value of the pseudo-second-order kinetic model was closer to 1, and its calculated q_e aligned more closely with the experimental data compared with pseudo-first-order kinetic. These findings indicated that the adsorption process was more consistent with the pseudo-second-order kinetic model, thereby providing evidence for the existence of chemisorption, such as ion exchange, inner-sphere complexation, and pore filling (Song et al. 2020; Maged et al. 2023b). Furthermore, the estimated adsorption rate in the initial 25 min of Mg-La LDH was calculated based on the experimental data. The calculated values were 34.0, 41.2, and 70.0 mg/(g·h), for LDH-2, LDH-3, and LDH-4, respectively. The obtained value of LDH-4 was 2.05 and 1.70 times than that of LDH-2 and LDH-3. These results explained the faster initial adsorption of LDH-4 compared to LDH-2 or LDH-3.

As for the intraparticle diffusion model, Fig. 5d exhibited three distinct stages during the adsorption process without origin, indicating that the in-particle diffusion process was not the only limiting factor during phosphate adsorption but also affected by external surface adsorption and boundary layer diffusion (Qiao et al. 2022; Jung et al. 2019). In the first stage, the three LDH fitting intercepts were smaller, indicating that the boundary layer thickness was thinner and the surface mass transfer opportunity was larger. Compared with LDH-2 and LDH-3, LDH-4 had a larger slope, indicating that there were more adsorption sites on the surface of LDH-4, thus providing a driving force for promoting adsorption and faster removal of phosphate (Li et al. 2021b; Seftel et al. 2018). In the second stage, the surface site had been occupied at this time, and the main process was that phosphate penetrates the internal pores of the adsorbent, which was affected by the intra-granular diffusion mechanism (Zhang et al. 2021b; Li et al. 2021b). With the increasing diffusion resistance of the inner hole, the adsorption enters the final stage. At this time, the dynamic equilibrium process of adsorption-desorption mainly occurred. Therefore, based on these results, the adsorption of P onto these LDHs was dominated by the chemical process, and the LDH-4 exhibited faster adsorption kinetics than others.

Table 2 Simulation parameters of pseudo-first-order, pseudo-second-order, and intraparticle diffusion models for phosphate adsorption by Mg-La LDH in wastewater

Kinetic model	Parameter	LDH-2	LDH-3	LDH-4
Pseudo-first-order model	R^2	0.581	0.676	0.786
	k_1 (min^{-1})	0.0537	0.0855	0.3336
	q_e (mg/L)	16.76	15.02	6.76
Pseudo-second-order mode	R^2	0.998	0.999	0.999
	k_2 (g/(mg·min))	0.098	0.0871	0.271
	q_e (mg/L)	16.10	19.52	25.12
Intra-particle diffusion mode	R_1^2	0.984	0.971	0.968
	K_1 (mg/(g·$h^{1/2}$))	14.96	17.33	29.57
	R_2^2	0.990	0.999	0.955
	K_2 (mg/(g·$h^{1/2}$))	1.73	2.37	1.84
	R_3^2	0.975	0.932	0.886
	K_3 (mg/(g·$h^{1/2}$))	0.86	0.89	0.26

Adsorption isotherms

In order to investigate the maximum adsorption capacity of these LDH adsorbents, adsorption experiments were conducted with different initial phosphate concentrations, and the obtained data were fitted by Langmuir and Freundlich isotherm models. As shown in Fig. 6, with the initial concentration increased, the adsorption capacity of these LDH also increased. Meanwhile, only LDH-4 showed a sharp increasing trend in adsorption capacity. The adsorption capacity of LDH-4 surged to around 85 mg/g with nearly no phosphate remaining in the solution. When the initial concentration of phosphate solution reached above 35 mg/L, the adsorption capacity of LDH-4 almost did not increase anymore. This observation indicated that the substantial P adsorption performance of LDH-4 was achieved by its superior adsorption performance rather than the high surrounding P concentration. However, in comparison, the LDH-2, LDH-3, and the common LDHs exhibited considerably slower and smoother curves of adsorption capacity: their adsorption capacities increased gradually with the higher initial concentrations. Therefore, the commendable performance of LDH-4 was not only about its higher adsorption capacity but also its extremely low equilibrium P concentration. This advantage would be perfectly suited to real situations and facilitate its applications.

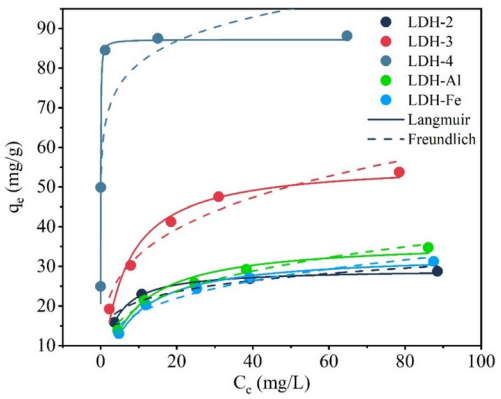

Fig. 6 Phosphate adsorption isotherms of Mg-La LDH simulated by the Langmuir and Freundlich models

As for the fitting results of Langmuir and Freundlich isotherms (Table 3), the R^2 values of the Langmuir model of the three LDHs were closer to 1, indicating a better fitting with the Langmuir model and suggesting a uniform single-layer adsorption process (Lin and Chen 2021). Through Langmuir fitting, the maximum adsorption capacities (q_{max}) of the three LDHs were determined as 29.29 mg/g, 56.29 mg/g, and 87.23 mg/g, respectively. The adsorption capacity of LDH-4 was 2.98 and 1.55 times higher than LDH-2 and LDH-3, confirming a positive effect can be achieved by increasing the molar ratio of Mg to La during Mg-La LDH synthesis. Additionally, R_L in the Langmuir model was calculated as 0.238, 0.371, and 0.003 for each LDH sample respectively, all of them were between 0 and 1. These indicated that phosphate could be effectively adsorbed onto LDHs and the adsorption was mainly chemisorption, which was consistent with the conclusions from kinetic results. These findings also suggested the favorability of the sorption process and implied a strong binding between Mg-La LDH and P (Wakejo et al. 2024). Moreover, a more representative value, $q_{0.5}$, which described the P adsorption capacity of the adsorbents with equilibrium P concentration at 0.5 mg/L, was calculated based on the Langmuir isotherm. The calculated values were 4.04, 4.41, and 81.96 mg/g, for LDH-2, LDH-3, and LDH-4, respectively. The obtained $q_{0.5}$ value of LDH-4 was 20.29 and 18.59 times that of LDH-2 and LDH-3. These results confirmed the superior performance of LDH-4 over others in the potential applications of real wastewater.

To compare the maximum phosphate adsorption capacity of the Mg-La LDH under study, Table 4 presented these data with the maximum phosphate adsorption capacity by researchers who investigated the removal of P using different LDHs. The results demonstrated that there was a great potential for LDH adsorbents to enhance phosphate adsorption by using La as the component metal in LDH synthesis.

Effect of pH

During the adsorption process, pH is the most important factor that affects the adsorption performance. The pH condition not only determines the predominant phosphate species in the solution but also affects the surface charge of the adsorbent. Therefore, the effect of initial pH conditions was investigated in this study.

As shown in Fig. 7, the adsorption effects of the three LDHs were all affected by pH, wherein a decrease in adsorption capacity with increasing pH within the range of 3 to 11 could be observed. Notably, the adsorption effects of LDH-2 and LDH-3 showed a higher sensitivity to pH change compared to LDH-4. Compared to alkaline conditions, the adsorption performance under acidic conditions of LDH-2 and LDH-3 was considerably better. This was mainly due to the poor crystallinity or malformation of the metal hydroxide layer. All of them would lead to the weakening of LDH ion exchange capacity. The adsorption effect of LDH-2 and LDH-3 were significantly influenced by solution pH also due to the higher difficulty for CO_3^{2-} anions in the LDH layer to undergo ion exchange compared to OH^-. It was further demonstrated that the performance of LDH synthesized at the Mg/La ratio of 4:1 exhibited superior performance. The adsorption efficiency of LDH-4 exhibited a slight decline with increasing pH. At pH 7.5, the predominance of $H_2PO_4^-$ in the solution shifted towards HPO_4^{2-}, which was unfavorable for ion exchange with LDH (Ashekuzzaman and Jiang 2017). Moreover, as the pH increased, the positive surface charge of the adsorbent gradually diminished. When pH > pH_{pzc} was applied, the surface of the adsorbent became negatively charged and produced electrostatic repulsion with phosphate ions (Jiang et al. 2019). The slight decrease in the adsorption effect also indicated that electrostatic attraction is not the main adsorption mechanism of LDH-4.

Effect of co-existing anions

The presence of co-existing anions has been demonstrated to result in competition with phosphate for active sites,

Table 3 Fitting parameters of isotherm models for phosphate adsorption by Mg-La LDH in wastewater

Absorbent	Langmuir				Freundlich		
	q_m (mg/g)	K_L (L/mg)	R_L	R^2	K_F (mg/g)	n	R^2
LDH-2	29.29	0.32	0.238	0.995	14.57	6.19	0.898
LDH-3	56.29	0.17	0.371	0.974	17.87	3.79	0.954
LDH-4	87.23	31.09	0.003	0.991	64.69	9.89	0.781
LDH-Al	36.46	0.12	0.45	0.975	10.38	3.61	0.974
LDH-Fe	33.15	0.12	0.44	0.989	9.97	3.79	0.955

Table 4 Comparison of phosphate adsorption capacity of the adsorbents applied in the present study and reported in the literature

Absorbent	Reaction conditions	Maximum adsorption capacity of the adsorbent (mg/g)	References
LDH-2	Absorbent dosage: 0.4 g/L Initial concentrations: 10–100 mg/L	29.29	This study
LDH-3	Absorbent dosage: 0.4 g/L Initial concentrations: 10–100 mg/L	56.29	This study
LDH-4	Absorbent dosage: 0.4 g/L Initial concentrations: 10–100 mg/L	87.23	This study
Mg-Al-CO_3 LDH-Chitosan composite	Absorbent dosage: 0.3 g/L Initial concentrations: 10–120 mg/L	106.35	(Isidoro Ribeiro et al. 2023)
Mg-Al-CO_3 LDH	Absorbent dosage: 0.3 g/L Initial concentrations: 10–120 mg/L	54.9	(Isidoro Ribeiro et al. 2023)
Mg-Al-CO_3 LDH	Absorbent dosage: 0.1 g/L Initial concentrations: 0.5–10 mg/L	31.3	(Yang et al. 2014)
Mg-Fe-LDH/BC	Absorbent dosage: 0.5 g/L Initial concentrations: 5–80 mg/L	50.6	(Zhang et al. 2021a)
Mg-Al-LDH/BC	Absorbent dosage: 0.5 g/L Initial concentrations: 5–80 mg/L	35.2	(Zhang et al. 2021a)
F-LDH	Absorbent dosage: 0.5 g/L Initial concentrations: 5–80 mg/L	58.8	(Feng et al. 2022a)
O-LDH	Absorbent dosage: 0.5 g/L Initial concentrations: 5–80 mg/L	36.8	(Feng et al. 2022a)

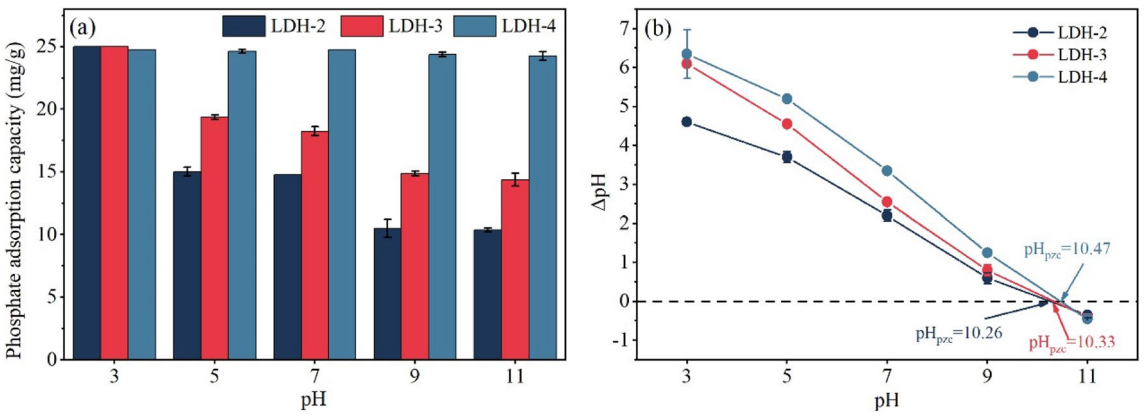

Fig. 7 (a) Effect of solution pH on adsorption and (b) measurement of pH_{pzc}

either through electrostatic attraction or complex formation, thereby influencing the adsorption process of adsorbents. Based on the aforementioned analysis, LDH-4 exhibited superior performance and was chosen for further investigations.

As given in Fig. 8, the effect of different co-existing anions on P adsorption onto LDH-4 was revealed. The presence of Cl^-, NO_3^-, and SO_4^{2-} had minimal influence on phosphate adsorption, whereas CO_3^{2-} had a significant impact on the adsorption. The presence of CO_3^{2-} in water altered the solution pH, causing the pH to rise and resulting in a decrease in the adsorption performance of LDH. Furthermore, anions would be enriched at the surface of the adsorbent through electrostatic interaction and then formed complexes where the co-existing anions and phosphates competed for positive attachment sites (Li et al. 2021a). Therefore, CO_3^{2-} had a strong binding ability that affects the adsorption effect of LDH on phosphates. However, even when the concentration of CO_3^{2-} reached 20 mM, only a marginal decrease (12.30%) in phosphate removal capacity was observed. These findings demonstrated that LDH-4 displayed a remarkable selectivity

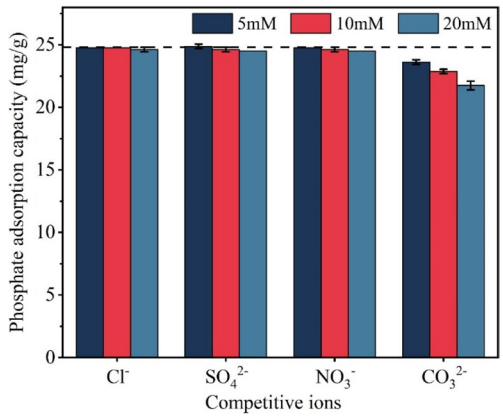

Fig. 8 Effects of co-existing anions with different concentrations on the adsorption of phosphate

towards phosphate and was particularly suitable for real wastewater treatment.

Study on desorption regeneration of the LDHs

The recycling performance of adsorbents is an important parameter to evaluate its potential in real wastewater treatment, as it can significantly reduce the costs in practical applications. In this study, 1 M Na_2CO_3 solution was used for regeneration. The adsorbed LDH was placed into a conical flask containing eluent and regenerated for 2 h at 25 °C to release pollutants and then used to remove phosphate. As illustrated in Fig. 9, it was observed that the utilization of 1.0 M Na_2CO_3 for desorption resulted in a desorption efficiency exceeding 80%. After 8 sorption-desorption cycles, the phosphorus removal efficiency decreased from 99.65 to 60.50%. The decrease in adsorption capacity may be related to the presence of an irreversible active adsorption site, specifically the strong complexation between metal cations and phosphates during the regeneration process (Zhang et al. 2021a; Wu et al. 2019). Under adsorption conditions, phosphate was adsorbed by ion exchange and complexation mechanisms. During the desorption process, excess CO_3^{2-} would diminish the affinity between Mg-La LDH and phosphate, facilitating the successful release of the phosphate. Specifically, P adsorbed through ion exchange could be effectively desorbed using Na_2CO_3, while P removed via complexation exhibited a higher resistance to desorption. Several cycle experiments showed that the adsorption rate remained at 60.50% and the desorption efficiency remained above 80%, thereby fully indicating that the Mg-La LDH prepared in this study had excellent recycling ability.

Adsorption mechanism

The SEM images of Mg-La LDH before and after adsorption are presented in Fig. 10 (a, b). After phosphate adsorption (Fig. 10b), the structure of Mg-La LDH remained intact while the surface smoothness decreased. Additionally, crystal characteristics became evident on the surface and the number of pores decreased, which could be attributed to phosphorus adsorption on the LDH surface.

The N_2 adsorption/desorption isotherm of Mg-La LDH before and after adsorption is shown in Fig. 10 (c, d), respectively. The isotherm was typical type IV, and the hysteresis loop was type H3, which was characteristic of mesoporous materials (Liu et al. 2019; Burtch et al. 2014). The results indicated that Mg-La LDH had a layered structure and the typical fissure pores were formed by the aggregation of nanoplates. The specific surface area of Mg-La LDH decreased from 134.01 to 87.11 m^2/g, and the total pore volume decreased from 0.23 to 0.16 cm^3/g. This was because P was adsorbed on the surface of the adsorbent and complexed with LDH metal ions, resulting in partial pore blockage on the surface. It was further proved that more adsorption sites

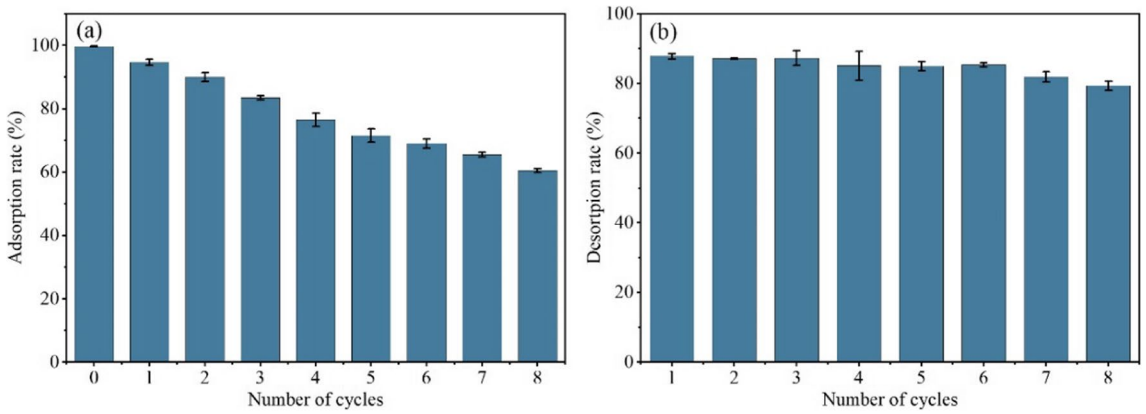

Fig. 9 Changes of adsorption rate (**a**) and desorption rate (**b**) in the recycling of phosphate adsorption by LDH

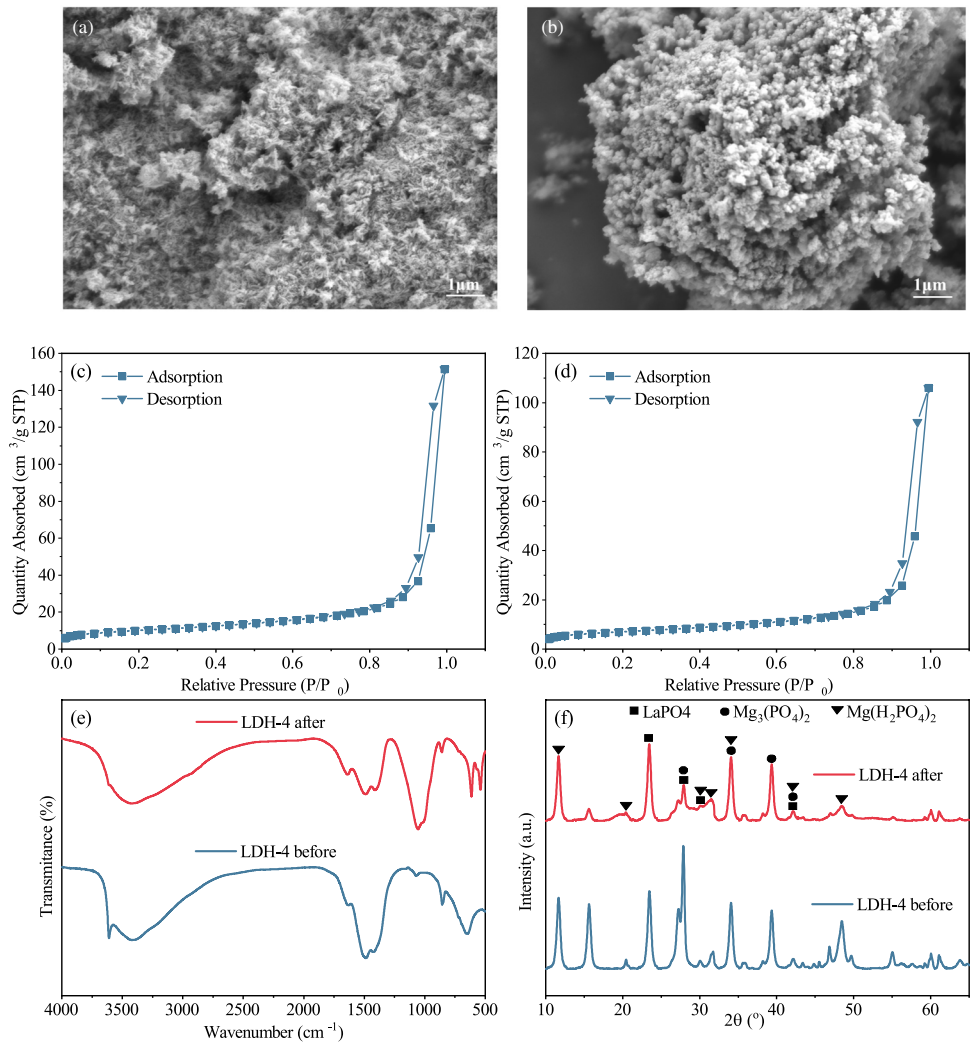

Fig. 10 SEM images of Mg-La LDH (**a**) and Mg-LDH+P (**b**), the N_2 adsorption-desorption isotherm of Mg-La LDH (**c**) and Mg-La LDH+P (**d**), and FTIR spectra (**e**) and XRD patterns (**f**) of Mg-La LDH and Mg-La LDH+P

provided by high specific surface area and pore volume were conducive to the improvement of adsorption capacity.

The FTIR spectra (Fig. 10e) confirmed the involvement of inner-sphere complexation in the adsorption process. The disappearance of OH on the surface of Mg-La LDH at 3698 cm^{-1} indicated the ion exchange between Mg-La LDH and phosphate in solution. Apart from the -OH group on the surface, the hydroxide and carbonate ions within the interlayer also participated in the phosphate adsorption in the form of ion exchange. The weakening or disappearance of hydroxyl at 1439 cm^{-1} and carbonate vibrations at 856 cm^{-1} could prove that they were involved in ion exchange processes. Additionally, a significantly weakened intensity was observed for M-O and M-O-M (M represents Mg or La) bands on the adsorbed LDH at 651 cm^{-1}, indicating that functional groups associated with M-O and M-O-M participated in the adsorption mechanism (Wu et al. 2018). A new band at 1053 cm^{-1} corresponded to the v_3 stretching vibration of phosphate and 538–614 cm^{-1} corresponded to the bending vibration of P-O (v_4), confirming the formation of M-O-P spherical complexation on the surface of Mg-La LDH (He et al. 2015; Li et al. 2023).

The XRD pattern of Mg-La LDH before and after adsorption is shown in Fig. 10f. The XRD patterns also demonstrated the role of ion exchange and inner-sphere complexation in adsorption. The high similarity of the main diffraction peaks of Mg-La LDH before and after adsorption indicated that the main crystal structure of LDH barely changed after adsorption. However, the diffraction peaks associated with Mg-La LDH after adsorption exhibited varying degrees of shift towards lower angles, which was due to the anion exchange between the interlayer anions and phosphate ions (Feng et al. 2022a). The movement of 2θ to a smaller angle also indicated that the Mg-La LDH surface spacing increased after phosphate adsorption. The adsorbed Mg-La LDH is roughly matched with the crystalline phases associated with metal-bound phosphates ($LaPO_4$, $Mg(H_2PO_4)_2$, $Mg_3(PO_4)_2$), which indicated the inner-sphere complexation between M-OH and phosphates on the surface of Mg-La LDH.

In order to further clarify the adsorption mechanism of Mg-La LDH on phosphate, XPS analysis of LDH before and

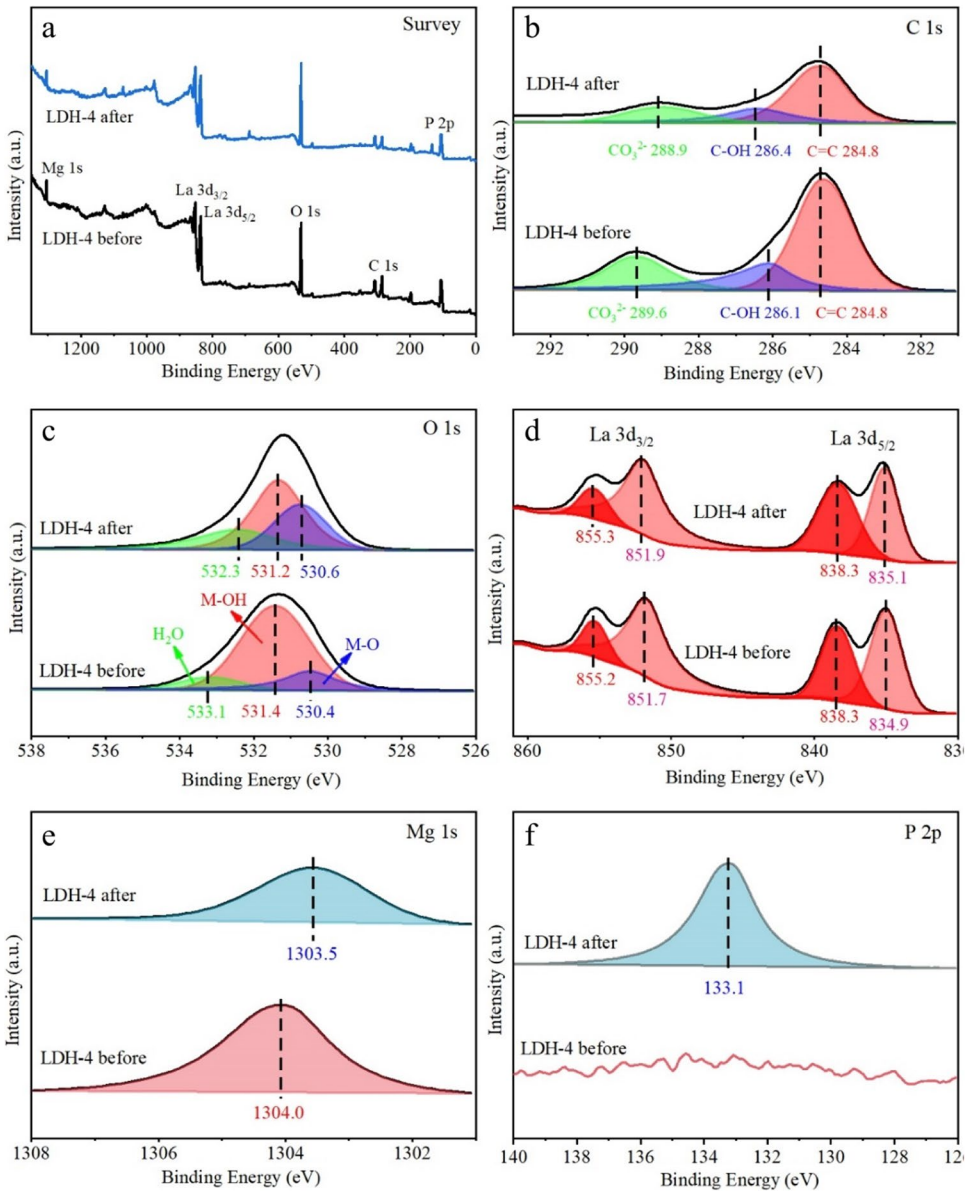

Fig. 11 XPS spectra of Mg-La LDH before and after adsorption: (**a**) XPS survey, (**b**) C 1s, (**c**) O 1s, (**d**) La 3d, (**e**) Mg 1s, and (**f**) P 2p

after adsorption was performed, and the results are shown in Fig. 11. Initially, four elements (Mg, La, C, O) were found in the survey scan of Mg-La LDH in Fig. 11a and an obvious P 2p peak appeared at approximately 133.1 eV after adsorption, indicating that phosphate was successfully adsorbed in LDH. The C 1s spectrum (Fig. 11b) was deconvolved into three peaks at 284.6 eV, 286.1 eV, and 289.6 eV corresponding to C-C, C-OH, and CO_3^{2-}, respectively. The proportion of CO_3^{2-} in total C 1s was significantly reduced after the adsorption process, which further indicated that CO_3^{2-} intercalation anion participated in phosphate adsorption. The convolution results of XPS O 1s spectra in Mg-La LDH are shown in Fig. 11c. Based on different forms of oxygen species, it can be divided into three peaks, M-O, M-OH, and H_2O (Xu et al. 2017). Among these peaks, M-O (530.4 eV) primarily corresponded to La-O and Mg-O bonds in the Mg-La LDH lattice, while M-OH (531.4 eV) is mainly related to Mg-OH and La-OH groups. The hydroxyl density of Mg-La LDH decreased significantly after phosphate adsorption, which further confirmed the interaction between phosphate and hydroxyl oxygen. Moreover, the energy position of La $3d_{3/2}$ and La $3d_{5/2}$ shifted by 0.2 eV after phosphate adsorption. The peak shift towards higher energy can be attributed to the transfer of electrons from the valence band of the ligand atom to the La atom's 4f orbital, suggesting the formation of a new P complex with La (Qu et al. 2020; Koh et al. 2020). In addition, there was a 0.5 eV shift towards lower binding energy in the Mg 1s XPS peak of Mg-La LDH, indicating that the adsorption site was extracted from the negatively charged phosphate O resulting in electron density (Gupta et al. 2020).

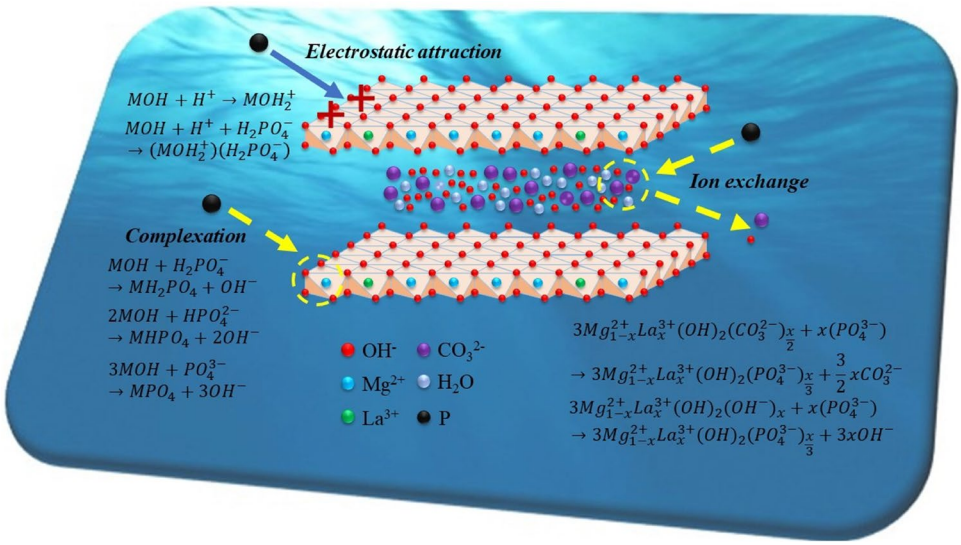

Fig. 12 Schematic diagram of possible phosphate adsorption mechanism of Mg-La LDH

According to the experimental results and characteristics mentioned above, three main mechanisms for the adsorption of phosphate by Mg-La LDH can be identified: (1) electrostatic attraction between phosphate and Mg-La LDH, (2) exchange of hydroxyl ions or carbonate ions between phosphate and Mg-La LDH, and (3) binds between phosphate and Mg-OH or La-OH to form monodentate complexes or bidentate complexes. The proposed mechanism is summarized in the Fig. 12.

Conclusion

A novel layered double hydroxide (LDH) with desirable characteristics and excellent performance in the removal of P from aqueous solutions was prepared using Mg and La as metal cations in this study. The optimum synthesis parameters of Mg-La LDH were obtained as follows: Mg:La = 4:1, synthesis temperature of 80 °C, synthesis pH of 10, and synthesis time of 10 h. The results of FTIR and XRD analysis confirmed that the Mg:La = 4:1 ratio was more favorable to crystal nucleation and growth, and Mg-La LDH with higher crystallinity could be synthesized. The adsorption kinetic study showed that 90% of the adsorption process of LDH-4 could be completed within the initial 60 min. The isotherm study showed that the maximum adsorption capacity of LDH-4 was 87.23 mg/g, and the adsorption capacity could reach 81.96 mg/g while only 0.50 mg/L of P remained in the solution, which was higher than most binary LDH adsorbents. The adsorption process was better fitted by the pseudo-second-order kinetic model and Langmuir model, indicating that the adsorption was a single-layer adsorption process dominated by chemisorption. The adsorption mechanism of P primarily includes electrostatic adsorption, ion exchange, and inner-sphere complexation. Due to the higher crystallinity and more complete structure of LDH-4, the adsorption of P was less affected by pH and different co-existing anions. Mg-La LDH regeneration experiment showed that even after undergoing eight repeated cycles of use, the phosphorus removal efficiency and desorption efficiency remained above 60.5% and 80%, respectively. In conclusion, Mg-La LDH exhibited significant potential for efficient phosphate adsorption in water treatment applications.

Author contribution Yanming Xu: conceptualization, methodology, investigation, formal analysis, visualization, and writing—original draft. Yue Yin: conceptualization, investigation, formal analysis, and writing—review and editing. Ya-Nan Luan: writing—review and editing. Qing Wang: Investigation, Methodology. Zhuo Zhao: Investigation, Methodology. Zhonghong Guo: Investigation, Methodology. Changqing Liu: supervision, funding acquisition, resources, writing—review and editing, and project administration.

Funding This study was funded by the Project of Qingdao Science and Technology Benefiting People Program (23-2-7-zdfn-2-nsh).

Data availability The data that support the findings of this study are available on request from the corresponding author, Changqing Liu.

Declarations

Ethical approval This study does not violate any ethical rules.

Consent to participate All authors agree to participate.

Consent for publication All authors agree to publish the article.

Competing interests The authors declare no competing interests.

References

Ahmed AAA, Talib ZA, bin Hussein MZ, Zakaria A (2012) Zn–Al layered double hydroxide prepared at different molar ratios: preparation, characterization, optical and dielectric properties. J Solid State Chem 191:271–278. https://doi.org/10.1016/j.jssc.2012.03.013

American Public Health Association-APHA (2017) Standard methods for the examination of water and wastewater, 23rd edn, Washington

Ashekuzzaman SM, Jiang J-Q (2017) Strategic phosphate removal/recovery by a re-usable Mg–Fe–Cl layered double hydroxide. Process Saf Environ Prot 107:454–462. https://doi.org/10.1016/j.psep.2017.03.009

Bukhtiyarova MV (2019) A review on effect of synthesis conditions on the formation of layered double hydroxides. J Solid State Chem 269:494–506. https://doi.org/10.1016/j.jssc.2018.10.018

Burtch NC, Jasuja H, Walton KS (2014) Water stability and adsorption in metal–organic frameworks. Chem Rev 114(20):10575–10612. https://doi.org/10.1021/cr5002589

Cavani F, Trifiro F, Vaccari AJCT (1991) Hydrotalcite-type anionic clays: preparation, properties and applications. Catal Today 11(2):173–301. https://doi.org/10.1016/0920-5861(91)80068-K

Chen D, Yin Y, Xu Y, Liu C (2023) Adsorptive recycle of phosphate by MgO-biochar from wastewater: adsorbent fabrication, adsorption site energy analysis and long-term column experiments. J Water Process Eng 51:103445. https://doi.org/10.1016/j.jwpe.2022.103445

Cordell D, Drangert J-O, White S (2009) The story of phosphorus: global food security and food for thought. Glob Environ Chang 19(2):292–305. https://doi.org/10.1016/j.gloenvcha.2008.10.009

Daud M, Hai A, Banat F, Wazir MB, Habib M, Bharath G, Al-Harthi MA (2019) A review on the recent advances, challenges and future aspect of layered double hydroxides (LDH) – containing hybrids as promising adsorbents for dyes removal. J Mol Liq 288:110989. https://doi.org/10.1016/j.molliq.2019.110989

Dox K, Everaert M, Merckx R, Smolders E (2019) Optimization of phosphate recovery from urine by layered double hydroxides. Sci Total Environ 682:437–446. https://doi.org/10.1016/j.scitotenv.2019.05.181

El-Qelish M, Maged A, Elwakeel KZ, Bhatnagar A, Elgarahy AM (2024) Dual valorization of coastal biowastes for tetracycline remediation and biomethane production: a composite assisted anaerobic digestion. J Hazard Mater 465:133143. https://doi.org/10.1016/j.jhazmat.2023.133143

Feng L, Zhang Q, Ji F, Jiang L, Liu C, Shen Q, Liu Q (2022a) Phosphate removal performances of layered double hydroxides (LDH) embedded polyvinyl alcohol / lanthanum alginate hydrogels. Chem Eng J 430:132754. https://doi.org/10.1016/j.cej.2021.132754

Feng X, Long R, Wang L, Liu C, Bai Z, Liu X (2022b) A review on heavy metal ions adsorption from water by layered double hydroxide and its composites. Sep Purif Technol 284:120099. https://doi.org/10.1016/j.seppur.2021.120099

Gupta NK, Saifuddin M, Kim S, Kim KS (2020) Microscopic, spectroscopic, and experimental approach towards understanding the phosphate adsorption onto Zn–Fe layered double hydroxide. J Mol Liq 297:111935. https://doi.org/10.1016/j.molliq.2019.111935

He JWW, Sun F et al (2015) Highly efficient phosphate scavenger based on well-dispersed $La(OH)_3$ nanorods in polyacrylonitrile nanofibers for nutrient-starvation antibacteria. ACS Nano 9(9):9292–9302. https://doi.org/10.1021/acsnano.5b04236

Iqbal MA, Fedel M (2018) The effect of the surface morphologies on the corrosion resistance of in situ growth MgAl-LDH based conversion film on AA6082. Surf Coat Technol 352:166–174. https://doi.org/10.1016/j.surfcoat.2018.08.006

Jiang YH, Li AY, Deng H, Ye CH, Li Y (2019) Phosphate adsorption from wastewater using ZnAl-LDO-loaded modified banana straw biochar. Environ Sci Pollut Res Int 26(18):18343–18353. https://doi.org/10.1007/s11356-019-05183-1

Jung K-W, Lee SY, Choi J-W, Lee YJ (2019) A facile one-pot hydrothermal synthesis of hydroxyapatite/biochar nanocomposites: adsorption behavior and mechanisms for the removal of copper(II) from aqueous media. Chem Eng J 369:529–541. https://doi.org/10.1016/j.cej.2019.03.102

Koh KY, Zhang S, Paul Chen J (2020) Hydrothermally synthesized lanthanum carbonate nanorod for adsorption of phosphorus: material synthesis and optimization, and demonstration of excellent performance. Chem Eng J 380:122153. https://doi.org/10.1016/j.cej.2019.122153

Koilraj P, Sasaki K (2017) Selective removal of phosphate using La-porous carbon composites from aqueous solutions: batch and column studies. Chem Eng J 317:1059–1068. https://doi.org/10.1016/j.cej.2017.02.075

Li A, Deng H, Wu Y, Ye C, Jiang Y (2021a) Strong adsorption of phosphorus by ZnAl-LDO-activated banana biochar: an analysis of adsorption efficiency, thermodynamics, and internal mechanisms. ACS Omega 6(11):7402–7412. https://doi.org/10.1021/acsomega.0c05674

Li H, Zhao Y, Xiao Z, Yang M, Zhou B (2021) Analysis on approximate site energy distribution and adsorption behaviors unveils reasons for highly efficient phosphorus removal by a novel sludge-based magnetic gel bead. Chem Eng J 422:130028. https://doi.org/10.1016/j.cej.2021.130028

Li S, Shao J, Ma B, Wu B, Hu C (2023) Oxygen defects of MgLa-LDH enhancing electrostatic attraction and inner-sphere complexation during phosphate adsorption from wastewater. Chem Eng J 464:142589. https://doi.org/10.1016/j.cej.2023.142589

Li Y, Wu M, Wu J, Wang Y, Zheng Z, Jiang Z (2022) Mechanistic insight and rapid co-adsorption of nitrogen pollution from micro-polluted water over MgAl-layered double hydroxide composite based on zeolite. Sep Purif Technol 297:121484. https://doi.org/10.1016/j.seppur.2022.121484

Lin J, He S, Wang X, Zhang H, Zhan Y (2019a) Removal of phosphate from aqueous solution by a novel $Mg(OH)_2/ZrO_2$ composite: adsorption behavior and mechanism. Colloids Surf A Physicochem Eng Asp 561:301–314. https://doi.org/10.1016/j.colsurfa.2018.11.001

Lin J, Wang X, Zhan Y (2019b) Effect of precipitation pH and coexisting magnesium ion on phosphate adsorption onto hydrous zirconium oxide. J Environ Sci 76:167–187. https://doi.org/10.1016/j.jes.2018.04.023

Lin Z, Chen J (2021) Magnetic Fe_3O_4@MgAl-LDH@$La(OH)_3$ composites with a hierarchical core-shell structure for phosphate removal from wastewater and inhibition of labile sedimentary phosphorus release. Chemosphere 264(Pt 2):128551. https://doi.org/10.1016/j.chemosphere.2020.128551

Liu C, Zhang M, Pan G, Lundehøj L, Nielsen UG, Shi Y, Hansen HCB (2019) Phosphate capture by ultrathin MgAl layered double hydroxide nanoparticles. Appl Clay Sci 177:82–90. https://doi.org/10.1016/j.clay.2019.04.019

Liu X, Fu J, Tang Y, Smith RL Jr, Qi X (2021) Mg-coordinated self-assembly of MgO-doped ordered mesoporous carbons for selective recovery of phosphorus from aqueous solutions. Chem Eng J 406:126748. https://doi.org/10.1016/j.cej.2020.126748

Maged A, Elgarahy AM, Haneklaus NH, Gupta AK, Show PL, Bhatnagar A (2023a) Sustainable functionalized smectitic clay-based nano hydrated zirconium oxides for enhanced levofloxacin sorption from aqueous medium. J Hazard Mater 452:131325. https://doi.org/10.1016/j.jhazmat.2023.131325

Maged A, Elgarahy AM, Hlawitschka MW, Haneklaus NH, Gupta AK, Bhatnagar A (2023b) Synergistic mechanisms for the superior sorptive removal of aquatic pollutants via functionalized biochar-clay composite. Bioresour Technol 387:129593. https://doi.org/10.1016/j.biortech.2023.129593

Ookubo A, Ooi K, Hayashi H (1992) Hydrotalcites as potential adsorbents of intestinal phosphate. J Pharm Sci 81(11):1139–1140. https://doi.org/10.1002/jps.2600811120

Qiao C-L, Xu Y-M, Yin Y, Xu Y-X, Xiao Y-H, Liu C-Q (2022) Adsorption of methyl orange on ZnO supported by seawater modified red mud. Water Sci Technol 85(7):2208–2224. https://doi.org/10.2166/wst.2022.102

Qu J, Akindolie MS, Feng Y, Jiang Z, Zhang G, Jiang Q, Deng F, Cao B, Zhang Y (2020) One-pot hydrothermal synthesis of NaLa(CO3)2 decorated magnetic biochar for efficient phosphate removal from water: kinetics, isotherms, thermodynamics, mechanisms and reusability exploration. Chem Eng J 394:124915. https://doi.org/10.1016/j.cej.2020.124915

Ribeiro NI, Pessanha OB, Pessanha ML, Guimarães D (2023) Efficient phosphate adsorption by a composite composed of $Mg_6Al_2(CO_3)(OH)_{16}$·4H2O LDH and chitosan: kinetic, thermodynamic, desorption, and characterization studies. Sep Purif Technol 307:122717. https://doi.org/10.1016/j.seppur.2022.122717

Santos LC, da Silva AF, Dos Santos Lins PV, da Silva Duarte JL, Ide AH, Meili L (2020) Mg-Fe layered double hydroxide with chloride intercalated: synthesis, characterization and application for efficient nitrate removal. Environ Sci Pollut Res Int 27(6):5890–5900. https://doi.org/10.1007/s11356-019-07364-4

Santosa SJ, Kunarti ES, Karmanto (2008) Synthesis and utilization of Mg/Al hydrotalcite for removing dissolved humic acid. Appl Surf Sci 254(23):7612–7617. https://doi.org/10.1016/j.apsusc.2008.01.122

Seftel EM, Ciocarlan RG, Michielsen B, Meynen V, Mullens S, Cool P (2018) Insights into phosphate adsorption behavior on structurally modified ZnAl layered double hydroxides. Appl Clay Sci 165:234–246. https://doi.org/10.1016/j.clay.2018.08.018

Shin EW, Han JS, Jang M, Min SH, Park JK, Rowell RM (2004) Phosphate adsorption on aluminum-impregnated mesoporous silicates: surface structure and behavior of adsorbents. Environ Sci Technol 38(3):912–917. https://doi.org/10.1021/es030488e

Song N, Xu J, Cao Y, Xia F, Zhai J, Ai H, Shi D, Gu L, He Q (2020) Chemical removal and selectivity reduction of nitrate from water by (nano) zero-valent iron/activated carbon micro-electrolysis. Chemosphere 248:125986. https://doi.org/10.1016/j.chemosphere.2020.125986

Tang N, He T, Liu J, Li L, Shi H, Cen W, Ye Z (2018) New insights into CO_2 adsorption on layered double hydroxide (LDH)-based nanomaterials. Nanoscale Res Lett 13:1–7. https://doi.org/10.1186/s11671-018-2471-z

Wakejo WK, Maged A, Meshesha BT, Kang JW, Demesa AG, Chakrabarti S, Bhaskar T, Gupta AK, Bhatnagar A (2024) Tuneable functionalized biochar for simultaneous removal of pharmaceuticals from binary mixture. Colloids Surf A Physicochem Eng Asp 681:132718. https://doi.org/10.1016/j.colsurfa.2023.132718

Wang B, Qu J, Li X, He X, Zhang Q, Riman R (2016) Precursor preparation to promote the adsorption of Mg-Al layered double hydroxide. J Am Ceram Soc 99(9):2882–2885. https://doi.org/10.1111/jace.14404

Wu D, Zhan Y, Lin J, Zhang Z, Xie B (2022) Contrasting effect of lanthanum hydroxide and lanthanum carbonate treatments on phosphorus mobilization in sediment. Chem Eng J 427:132021. https://doi.org/10.1016/j.cej.2021.132021

Wu P, Xia L, Liu Y, Wu J, Chen Q, Song S (2018) Simultaneous sorption of arsenate and fluoride on calcined Mg–Fe–La hydrotalcite-like compound from water. ACS Sustain Chem Eng 6(12):16287–16297. https://doi.org/10.1021/acssuschemeng.8b03209

Wu RS, Lam KH, Lee JM, Lau TC (2007) Removal of phosphate from water by a highly selective La(III)-chelex resin. Chemosphere 69(2):289–294. https://doi.org/10.1016/j.chemosphere.2007.04.022

Wu Y, Li X, Yang Q, Wang D, Xu Q, Yao F, Chen F, Tao Z, Huang X (2019) Hydrated lanthanum oxide-modified diatomite as highly efficient adsorbent for low-concentration phosphate removal from secondary effluents. J Environ Manag 231:370–379. https://doi.org/10.1016/j.jenvman.2018.10.059

Xiong W, Tong J, Yang Z, Zeng G, Zhou Y, Wang D, Song P, Xu R, Zhang C, Cheng M (2017) Adsorption of phosphate from aqueous solution using iron-zirconium modified activated carbon nanofiber: performance and mechanism. J Colloid Interface Sci 493:17–23. https://doi.org/10.1016/j.jcis.2017.01.024

Xu R, Zhang M, Mortimer RJ, Pan G (2017) Enhanced phosphorus locking by novel lanthanum/aluminum-hydroxide composite: implications for eutrophication control. Environ Sci Technol 51(6):3418–3425. https://doi.org/10.1021/acs.est.6b05623

Yang K, Yan LG, Yang YM, Yu SJ, Shan RR, Yu HQ, Zhu BC, Du B (2014) Adsorptive removal of phosphate by Mg–Al and Zn–Al layered double hydroxides: kinetics, isotherms and mechanisms. Sep Purif Technol 124:36–42. https://doi.org/10.1016/j.seppur.2013.12.042

Yang Y, Wang Y, Zheng C, Lin H, Xu R, Zhu H, Bao L, Xu X (2022) Lanthanum carbonate grafted ZSM-5 for superior phosphate uptake: investigation of the growth and adsorption mechanism. Chem Eng J 430:133166. https://doi.org/10.1016/j.cej.2021.133166

Yin Y, Xu G, Xu Y, Guo M, Xiao Y, Ma T, Liu C (2021) Adsorption of inorganic and organic phosphorus onto polypyrrole modified red mud: evidence from batch and column experiments. Chemosphere 286(Pt 3):131862. https://doi.org/10.1016/j.chemosphere.2021.131862

Zhang J, Xia Q, Hong X, Chen J, Liu D (2021) Synthesis of layered double hydroxides with nitrate and its adsorption properties of phosphate. Water Sci Technol 83(1):100–110. https://doi.org/10.2166/wst.2020.567

Zhang X, Song Z, Dou Y, Xue Y, Ji Y, Tang Y, Hu M (2021b) Removal difference of Cr(VI) by modified zeolites coated with MgAl and ZnAl-layered double hydroxides: efficiency, factors and mechanism. Colloids Surf A Physicochem Eng Asp 621:126583. https://doi.org/10.1016/j.colsurfa.2021.126583

Zhang Y, Qin J, Wang X, Chen Z, Zheng X, Chen Y (2021c) Advanced treatment of phosphorus-containing tail water by Fe-Mg-Zr layered double hydroxide beads: performance and mechanism. J Environ Manag 296:113–203. https://doi.org/10.1016/j.jenvman.2021.113203

Zou Y, Zhang R, Wang L, Xue K, Chen J (2020) Strong adsorption of phosphate from aqueous solution by zirconium-loaded Ca-montmorillonite. Appl Clay Sci 192:105638. https://doi.org/10.1016/j.clay.2020.105638

Zubair M, Daud M, McKay G, Shehzad F, Al-Harthi MA (2017) Recent progress in layered double hydroxides (LDH)-containing hybrids as adsorbents for water remediation. Appl Clay Sci 143:279–292. https://doi.org/10.1016/j.clay.2017.04.002